effects of weak 45–75 Hz electromagnetic fields on the slime mold physarum polycephalum," presented at the 1975 URSI Annual Meeting, Boulder, CO, Oct. 20–23, 1975 (Session B-10a).
[7] Arthur W. Guy, "5.0 objects in the fields," Rep. to National Council on Radiation Protection and Measurement, July 1975.
[8] H. P. Schwan and G. M. Piersol, "The absorption of electromagnetic energy in body tissues, pt. I," *Amer. J. Phys. Med.*, vol. 33, pp. 371–404, 1954.
[9] — —, "The absorption of electromagnetic energy in body tissues, pt. II," *Amer. J. Phys. Med.*, vol. 34, pp. 425–448, 1955.
[10] O. Ghandi, private communication.
[11] S. Ramo, J. R. Whinnery, and T. Van Duzer, *Fields and Waves in Communication Electronics*. New York: Wiley, 754 pp.
[12] S. Takashima, R. Yantorno, and N. C. Pal, "Electrical properties of squid axon membrane II: Effect of partial degradation by phospholipase A and pronase on electrical characteristics," *Biochimica et Biophysica Acta*, vol. 401, pp. 15–27, 1975.
[13] S. H. White and T. E. Thompson, "Capacitance, area and thickness variations in thin lipid films," *Biochimica et Biophysica Acta*, vol. 323, pp. 7–22, 1973.
[14] Gary J. Grimes and F. S. Barnes, "Chemotactic responses of human PMN's to cyclic GMP and other compounds," *Experimental Cell Research*, vol. 87, 1974.
[15] R. Caldwell, "Birefringence in macromolecular solutions," master's thesis, University of Colorado, 1976, unpublished.
[16] P. R. Brooks, "Reactions of oriented molecules," *Science*, vol. 193, no. 4247, pp. 11–24, July 2, 1976.
[17] D. McRee, R. H. Wyatt, J. K. Haseman, and G. Somjen, "The transmission of reflexes in the spinal cord of cats during direct irradiation with microwaves," *J. Microwave Power*, vol. 11, no. 1, pp. 49–60, 1976.
[18] H. Wachtel, R. Seaman, and W. Joines, "Effects of low-intensity microwaves on isolated neurons," *Annals New York Academy of Sciences*, vol. 247, pp. 46–62, Feb. 28, 1975.

Internal EM Field and Absorbed Power Density in Human Torsos Induced by 1–500-MHz EM Waves

KUN-MU CHEN, FELLOW, IEEE, AND BHAG S. GURU, MEMBER, IEEE

Abstract—**Numerical results on the internal electromagnetic (EM) field and absorbed power density inside a human torso induced by EM waves of frequencies ranging from 1 to 500 MHz and of both vertical and horizontal polarizations are presented. The induced fields inside the torso are shown to be dependent on the frequency and the torso geometry. Theoretical results are obtained based on the tensor integral equation method and some theoretical predictions are compared to existing experimental results.**

I. Introduction

In the study of biological effects induced by electromagnetic (EM) waves and in medical applications utilizing EM radiation, it is important and desirable to know the internal EM field and absorbed power density induced by an EM field inside a human torso.

The existing methods commonly used to predict the induced EM field inside a biological body are based on simplified models of a plane slab [1], [2], a sphere [3]–[5], a cylinder [6], and spheroids [7], [8]. Although these simple models provide estimates of the internal EM fields, the results have limited applicability to biological bodies with irregular shapes illuminated by an EM wave with a frequency higher than the VHF range.

This paper presents numerical results on the internal EM field and absorbed power density inside a human torso induced by EM waves of frequencies ranging from 1 to 500 MHz and of both vertical and horizontal polarizations. Numerical results are obtained based on a recently developed "tensor integral equation method" [9]. This method was found to be quite powerful in quantifying the induced EM field inside an arbitrarily shaped biological body such as a human torso.

The accuracy of this method has been verified theoretically by convergence tests [9] and experimentally by tests conducted in scaled models containing saline solution [10].

For the reader's benefit, the tensor integral equation method and its experimental verification are briefly outlined in Section II. Numerical results on the internal EM field and the absorbed power density in human torsos of various shapes induced by EM waves of various frequencies with different polarizations are presented in Section III.

II. The Theoretical Method and Its Accuracy

Since the tensor integral equation method [9] has been published, only two key equations are quoted here.

If a finite biological body of arbitrary shape, with permit-

Manuscript received May 18, 1976; revised February 23, 1977. This research was supported in part by NSF under Grant ENG 74-12603 and in part by the Army Office of Research under Grant DAAG 29-76-G-0201.

The authors are with the Department of Electrical Engineering and Systems Science, Michigan State University, East Lansing, MI 48824.

tivity $\varepsilon(r)$, conductivity $\sigma(\vec{r})$, and permeability μ_0, is illuminated in free space by an incident EM wave with electric field $\vec{E}^i(\vec{r})$, the total induced electric field $\vec{E}(\vec{r})$ inside the body can be determined from the following tensor integral equation:

$$\left[1+\frac{\tau(\vec{r})}{3j\omega\varepsilon_0}\right]\vec{E}(\vec{r})-PV\int_V \tau(\vec{r}')\vec{E}(\vec{r}')\cdot\overleftrightarrow{G}(\vec{r},\vec{r}')\,dV'=\vec{E}^i(\vec{r}) \quad (1)$$

where $\tau(\vec{r})=\sigma(\vec{r})+j\omega(\varepsilon(\vec{r})-\varepsilon_0)$, ε_0 is the free-space permittivity, the PV symbol means the principal value of the integral, $\overleftrightarrow{G}(\vec{r},\vec{r}')$ is the free-space tensor Green's function, and V is the body volume.

If the body is partitioned into N subvolumes or cells, and $\vec{E}(\vec{r})$ and $\tau(\vec{r})$ are assumed to be constant within each cell, equation (1) can be transformed into $3N$ simultaneous equations for E_x, E_y, and E_z at the centers of N cells by the point matching method. These simultaneous equations can be written into matrix form as

$$\begin{bmatrix}[G_{xx}] & [G_{xy}] & [G_{xz}]\\ [G_{yx}] & [G_{yy}] & [G_{yz}]\\ [G_{zx}] & [G_{zy}] & [G_{zz}]\end{bmatrix}\begin{bmatrix}[E_x]\\ [E_y]\\ [E_z]\end{bmatrix}=-\begin{bmatrix}[E_x^i]\\ [E_y^i]\\ [E_z^i]\end{bmatrix}. \quad (2)$$

The $[G]$ matrix is a $3N \times 3N$ matrix, while $[E]$ and $[E^i]$ are $3N$ column matrices expressing the total electric field and the incident electric field at the centers of N cells. The elements of the $[G]$ matrix have been evaluated in [9]. Therefore, with the known incident electric field $\vec{E}^i(\vec{r})$, the total induced electric field $\vec{E}(\vec{r})$ inside the body can be obtained from (2) by inverting the $[G]$ matrix.

In numerical analysis such as the present tensor integral equation method, it is important to establish an upper limit on the dimensions of the cells for the required accuracy. In [9], two convergence tests have been performed for this purpose, one in a muscle cylinder and the other in a muscle cube. It was found from these tests that reliable numerical results can be obtained if the cell edge does not exceed a quarter free-space wavelength.

Other factors which dictate the selection of the cell size are the computer storage capacity and the size of the biological body. Our numerical computation was performed with a CDC 6500 computer which has a maximum capacity of inverting a 120×120 matrix. This limits the maximum number of cells to 40. In this paper a typical adult torso of 1.7-m height is considered. When the symmetries between the right half and the left half and between the front layer and the back layer of the torso are assumed, for simplicity, a cell size of 10 cm^3 seems appropriate.

Once the 10-cm^3 cell size is adapted, the highest frequency we can consider without violating the criterion that the cell edge not exceed a quarter free-space wavelength is 750 MHz. However, to provide a safe margin of accuracy, we consider a frequency range with an upper bound of 500 MHz.

The validity of the theoretical method and the accuracy of the numerical results can be provided by experimental results. The results of two experiments are discussed below and are compared with corresponding theoretical results.

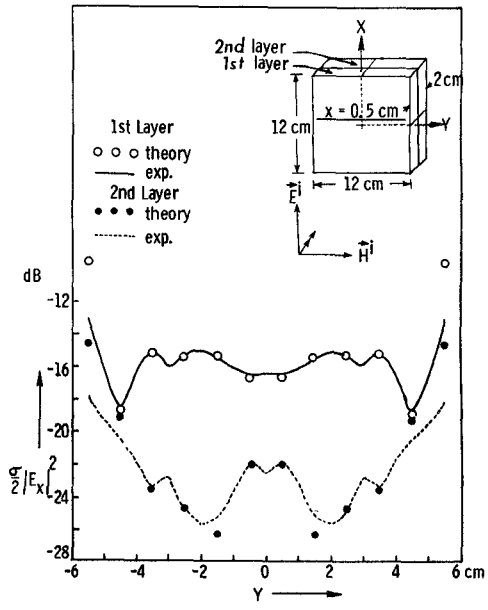

Fig. 1. Theoretical and experimental values of the dissipated power due to E_x, $(\sigma/2)|E_x|^2$, as a function of Y along $x = 0.5$ cm. Frequency = 2.45 GHz; $\sigma = 5.934$ ℧/m; $\varepsilon = 68.487\varepsilon_0$. Salt concentration = 0.5 normal.

Fig. 1 shows a comparison of theoretical and experimental results on the absorbed (dissipated) power in a 12- × 12- × 2-cm rectangular box containing 0.5-normal saline solution induced by a 2.45-GHz microwave with a vertical electric field incident normally upon the box. A conductivity of 5.93 ℧/m and a permittivity of $68.487\varepsilon_0$ were assumed for the saline solution at 2.45 GHz. In the numerical calculation, the box was divided into two layers and each layer was subdivided into 144-cm^3 cells. The induced electric field and absorbed power density were calculated at the center of each cell. In Fig. 1, theoretical and experimental results for the dissipated power due to the vertical component of the induced electric field E_x, which is determined as $\sigma/2\,|E_x|^2$ (σ is the conductivity), are plotted as a function of y along $x = 0.5$-cm lines passing through the centers of the first and second layers. The distribution pattern of the absorbed power density is, in general, quite complicated as shown in the figure. The absorbed power density in the first layer is several decibels higher than that in the second layer, as expected. An interesting observation, however, is that the distribution patterns of the absorbed power densities differ significantly in these two layers. Excellent agreement between the theory and experiment is observed except for a minor discrepancy at the very edges of the box. This discrepancy between the theory and experiment at the body edges is due to an inherent experimental error associated with an implantable field probe as discussed elsewhere [10].

Fig. 2(a) and (b) shows a comparison of the theoretical and experimental results on the absorbed power density in an I-shaped model, filled with a saline solution of 0.5 normality, induced by a 2.45-GHz microwave with a vertical electric field and at end-on incidence. The theoretical and experimental results for the absorbed power density due to the vertical component of the induced electric field E_x, $\sigma/2\,|E_x|^2$, as a function of y along $x = 3.5$-cm and

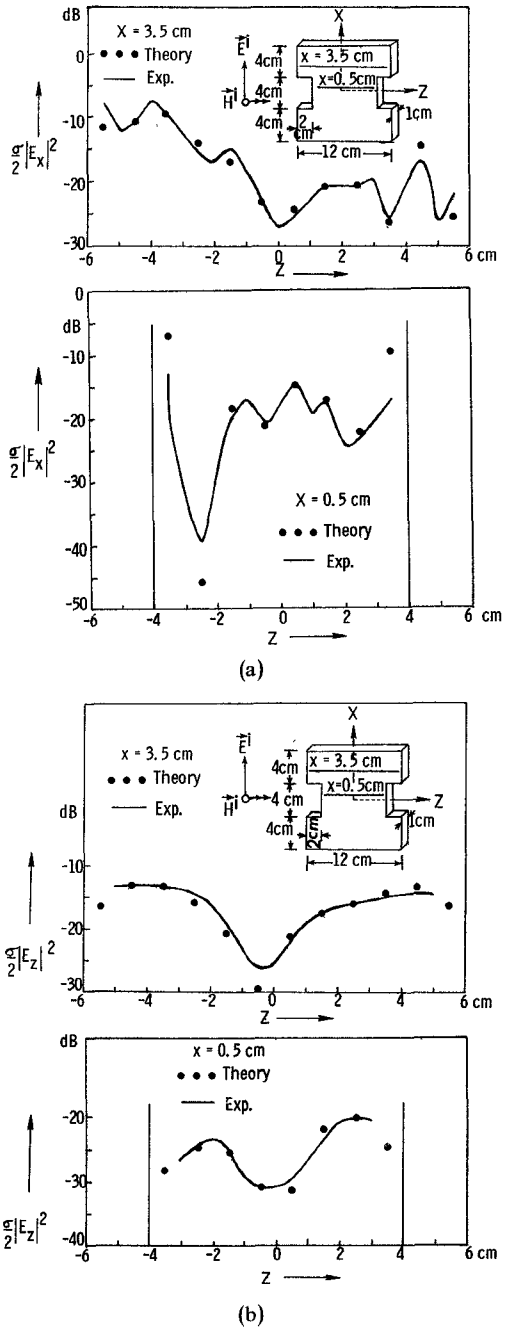

Fig. 2. (a) Theoretical and experimental values of the dissipated power due to E_x, $(\sigma/2)|E_x|^2$, as a function of Z along $x = 3.5$ cm and $x = 0.5$ cm. Frequency = 2.45 GHz; $\sigma = 5.934$ ℧/m; $\varepsilon = 68.487\varepsilon_0$. Salt concentration = 0.5 normal. (b) Theoretical and experimental values of the dissipated power due to E_z, $(\sigma/2)|E_z|^2$, as a function of Z along $x = 3.5$ cm and $x = 0.5$ cm. Frequency = 2.45 GHz; $\sigma = 5.934$ ℧/m; $\varepsilon = 68.487\varepsilon_0$. Salt concentration = 0.5 normal.

$x = 0.5$-cm lines are compared in Fig. 2(a). The patterns of the absorbed power densities are quite complicated functions of the location, but the agreement between the theoretical and experimental results is very good. Fig. 2(b) shows the theoretical and experimental results on the absorbed power density due to the horizontal component of the induced electric field E_z, $\sigma/2\,|E_z|^2$, as a function of y along $x = 3.5$-cm and $x = 0.5$-cm lines. Very good agreement between the theory and experiment is again observed in this figure except at the very edges of the model.

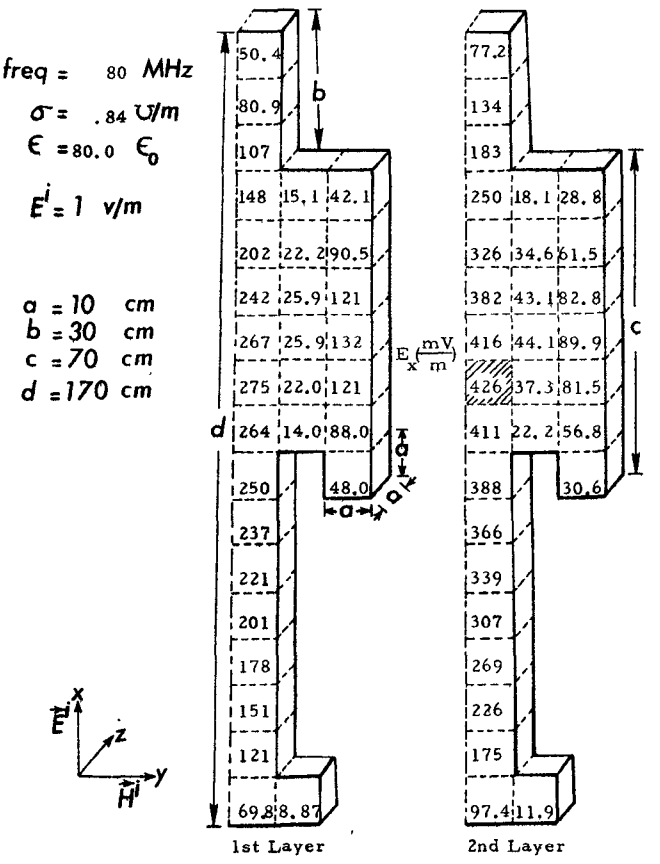

Fig. 3. The x component of an electric field induced inside a human torso by a vertically polarized EM wave of 80 MHz with an incident electric field of 1 V/m.

With the convergence tests and the experimental verification discussed above, we feel that the numerical results in the following sections should be quite reliable.

III. Induced Electric Field and Absorbed Power Density in Human Torsos

After the validity and accuracy of the tensor integral equation method were confirmed experimentally, this method was used to quantify the internal electric field and absorbed power density inside human torsos induced by incident EM waves of various frequencies, ranging from 1 to 500 MHz, with both vertical and horizontal polarizations. Extensive results have been summarized in [11]. For the sake of brevity, however, only a few examples are discussed in this paper.

A. Induced Electric Field and Absorbed Power Density in an Adult Torso

An adult torso with a height of 1.7 m and a shape as shown in Fig. 3 is considered. An EM wave of 80 MHz with either vertical or horizontal polarization is assumed to be incident normally upon the torso. A frequency of 80 MHz is chosen because at this frequency the torso exhibits a resonance phenomenon in response to a vertically polarized EM wave.

Fig. 3 shows the x component of the electric field induced by a vertically polarized EM wave of 80 MHz with an incident electric field of 1 V/m at normal incidence. In the

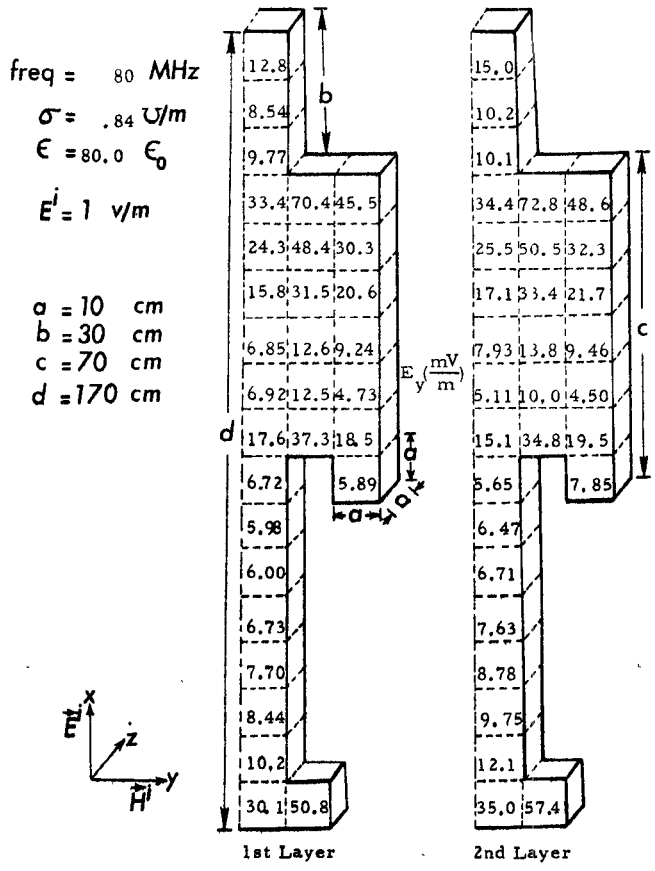

Fig. 4. The y component of an electric field induced inside a human torso by a vertically polarized EM wave of 80 MHz with an incident electric field of 1 V/m.

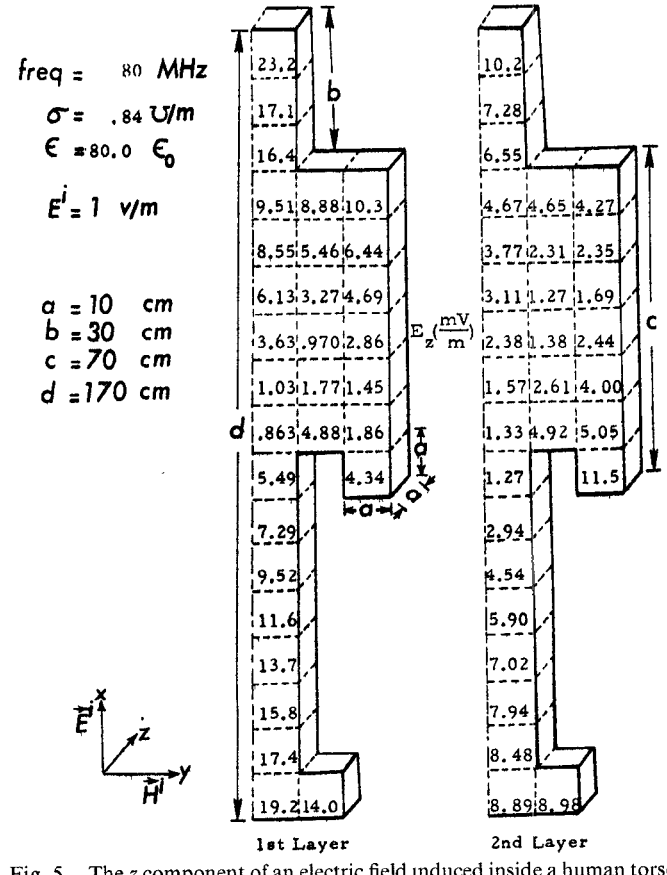

Fig. 5. The z component of an electric field induced inside a human torso by a vertically polarized EM wave of 80 MHz with an incident electric field of 1 V/m.

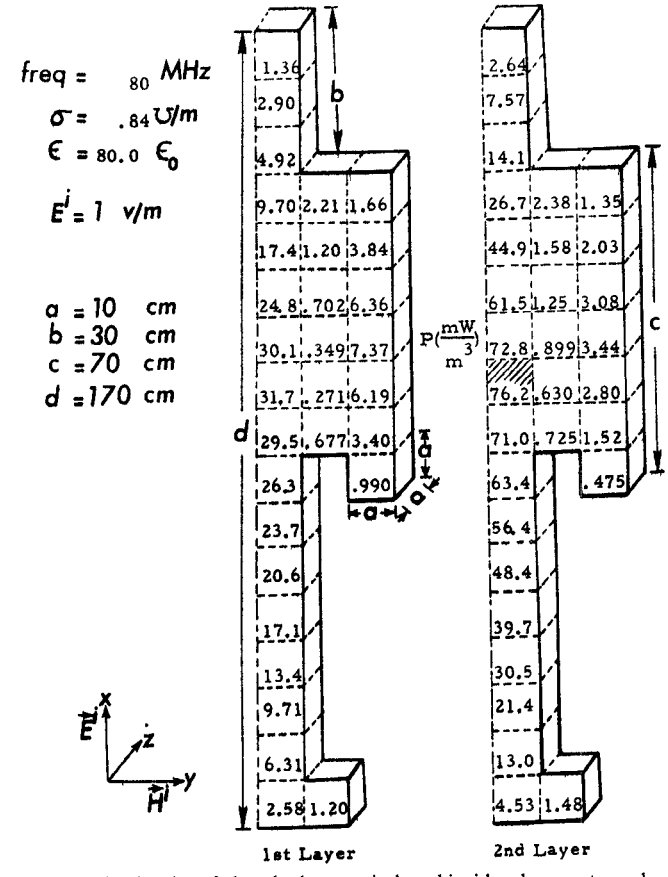

Fig. 6. The density of absorbed power induced inside a human torso by a vertically polarized EM wave of 80 MHz with an incident electric field of 1 V/m.

numerical calculation, the torso was divided into 124 ten-cubic-centimeter cells and the electric field was calculated at the centers of the cells. Due to symmetry, only half of the torso is shown. The strongest induced electric field is about 0.426 times the incident electric field and is located at the hatched area, as shown in Fig. 3. It is also noted that the induced fields in the front layer (the first layer) and in the back layer are quite different and that at 80 MHz the latter is stronger than the former over the major part of the torso. Figs. 4 and 5 show the y and z components of the induced electric field. Fig. 6 shows the corresponding absorbed power density given by $\sigma/2(E_x^2 + E_y^2 + E_z^2)$.

When the same torso is illuminated by a horizontally polarized EM wave of 80 MHz with a unity incident electric field, the strongest induced electric field is in the y direction, as expected. Figs. 7–9 show the x, y, and z components of the induced electric field, respectively. As shown in Fig. 8, the strongest induced electric field in the y direction is about 0.0622 times the incident electric field and is located at about the same area as in the case of vertical polarization. It is also noted that the induced electric field for the horizontal polarization case is generally smaller than that of the case of vertical polarization at 80 MHz. However, this will not be so at higher frequencies. This will be discussed later. The absorbed power density is shown in Fig. 10.

It is important to point out that from extensive results for various frequencies [11], it is observed that the value and

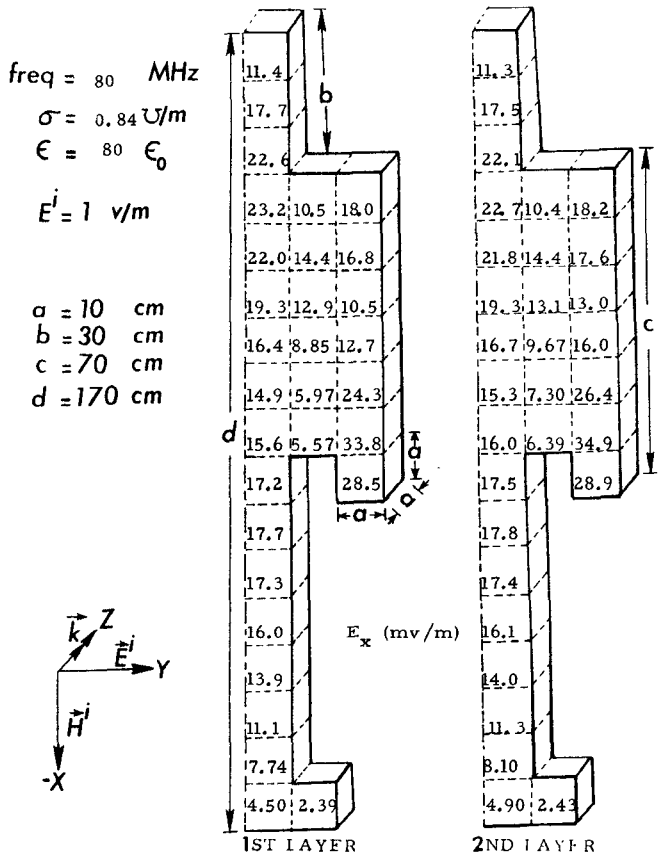

Fig. 7. The x component of an electric field induced inside a human torso by a horizontally polarized EM wave of 80 MHz with an incident electric field of 1 V/m.

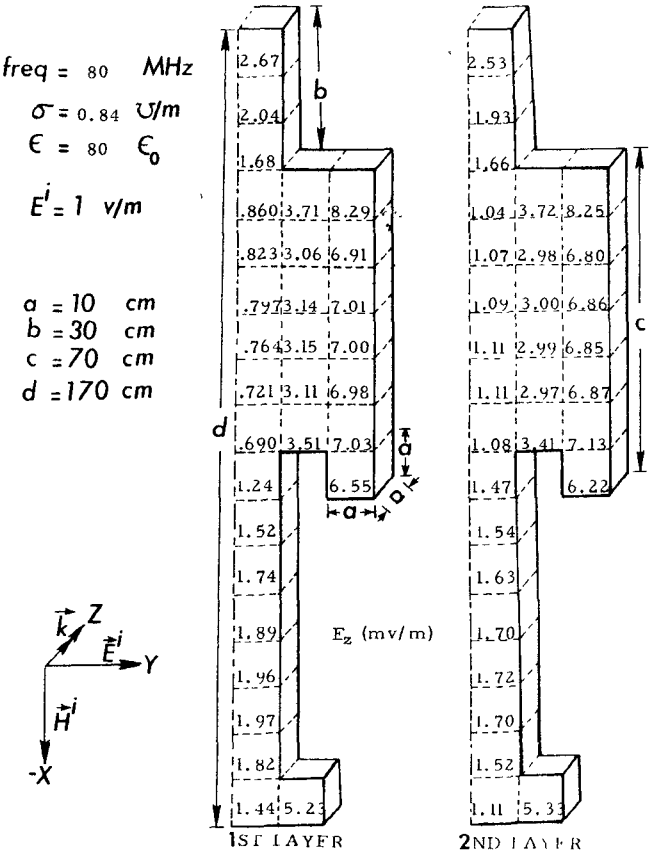

Fig. 9. The z component of an electric field induced inside a human torso by a horizontally polarized EM wave of 80 MHz with an incident electric field of 1 V/m.

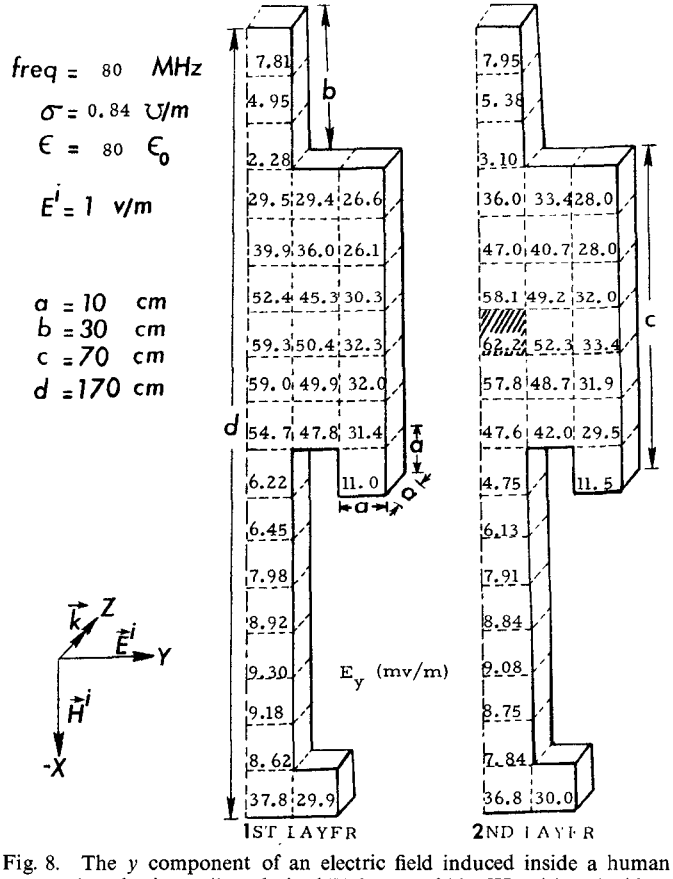

Fig. 8. The y component of an electric field induced inside a human torso by a horizontally polarized EM wave of 80 MHz with an incident electric field of 1 V/m.

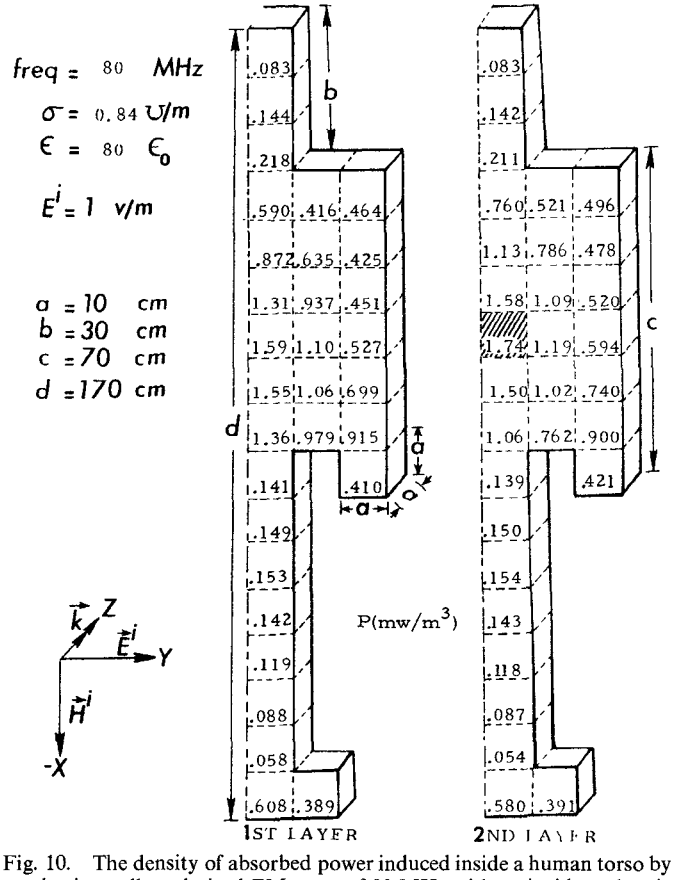

Fig. 10. The density of absorbed power induced inside a human torso by a horizontally polarized EM wave of 80 MHz with an incident electric field of 1 V/m.

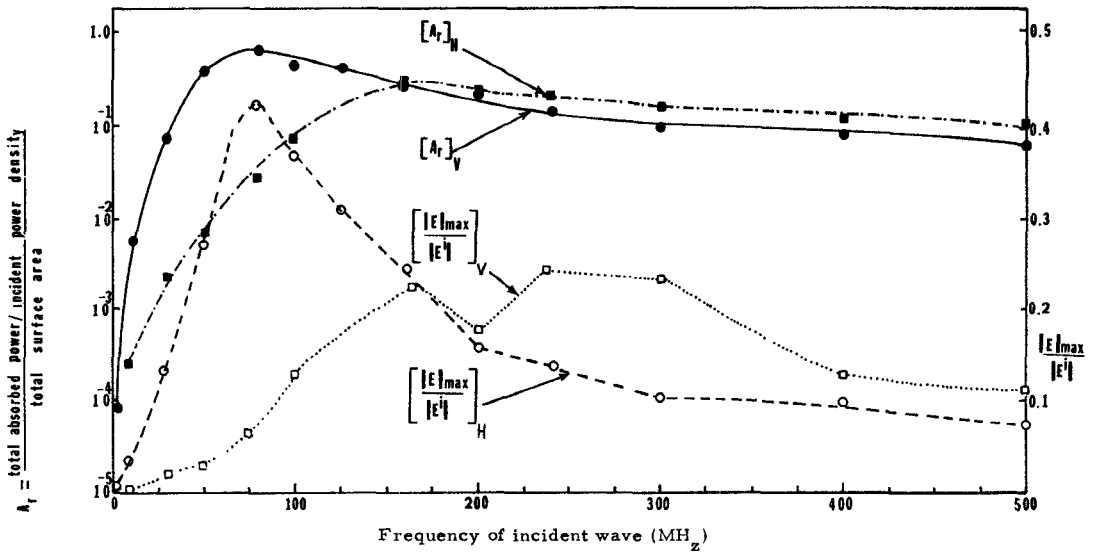

Fig. 11. Relative absorption area and relative maximum induced field in the torso of an adult 1.7 m in height as functions of the frequency of the vertically polarized and horizontally polarized incident EM waves.

location of the strongest induced electric field inside a human torso vary as functions of the frequency and polarization of the incident EM wave.

B. Maximum Induced Electric Field and Total Absorbed Power as Functions of Frequency

The results on an induced field in an adult torso 1.7 m in height over the frequency range of 1–500 MHz are summarized in Fig. 11. The total power absorbed by the torso is expressed in terms of the relative absorption area A_r, which is defined as [(total absorbed power/incident power density)/total torso surface area], because the heat dissipation capability of a human torso is essentially determined by the total surface area of the torso. The maximum induced electric field is represented by its value normalized by the incident electric field: $|E_{max}|/|E^i|$.

From Fig. 11 it is observed, for vertical polarization, that the normalized maximum induced electric field reaches a sharp maximum and the relative absorption area attains a weak peak at around 80 MHz. This implies that a resonance occurs in a human torso when the torso height is about 0.453 times the free-space wavelength of the incident EM wave.

For horizontal polarization, the induced electric field seems to have two local maxima at 170 and 230 MHz. At 230 MHz the maximum horizontal dimension of the torso is about 0.46 times the free-space wavelength of the incident EM wave and this may be considered as a resonance condition. The absorbed power for the horizontal polarization case tends to increase monotonically with the frequency first and then stay rather constant for frequencies higher than 170 MHz.

It is true at frequencies lower than 100 MHz that the induced field in an adult torso is much stronger for the vertical polarization case than for the horizontal polarization case. However, for frequencies higher than 170 MHz a horizontally polarized EM wave, in general, induces a stronger field than a vertically polarized EM wave inside a typical adult torso.

C. Induced Electric Field and Absorbed Power Density as Functions of Torso Geometry

The induced fields presented in Figs. 3–11 have been calculated inside a somewhat simplified human torso to facilitate the numerical computation. A recent experimental study by Gandhi [12] has shown that a hot spot can be created in the neck region of a simulated human model when it is illuminated by an EM wave with a frequency in the resonance region. This result tends to imply that absorbed power density can be enhanced at a narrowed region of a torso. To observe this phenomenon theoretically, and to examine the general effect of the torso geometry on the distributions of the induced electric field and absorbed power density inside the torso, three cases of modified torsos are considered.

The first modified torso is the previous torso with the neck region thinned as shown in Fig. 12. This modified torso is then illuminated by a vertically polarized EM wave of 80 MHz with a unity incident electric field. The induced electric field and absorbed power density are then calculated inside this modified torso. Figs. 12–15 show the x, y, and z components of the induced electric field and the absorbed power density in this modified torso. When these results are compared with the corresponding results in the previous torso with a thick neck, as shown in Figs. 3–6, it is observed that a local hot spot is indeed created in the thinned neck region, while the induced fields at other parts of the torso are only slightly altered from the previous case. Physically, this phenomenon is reasonable because the induced vertical current is now squeezed into the thinned neck region and the current density at the neck region is increased resulting in a local hot spot.

The second modified torso is the previous torso with outstretched arms as shown in Fig. 16. This torso is assumed to be illuminated by a vertically polarized EM wave of 30 MHz with a unity incident electric field. Figs. 16–18 show the x and y components of the induced electric field and the absorbed power density in this torso. The z component of

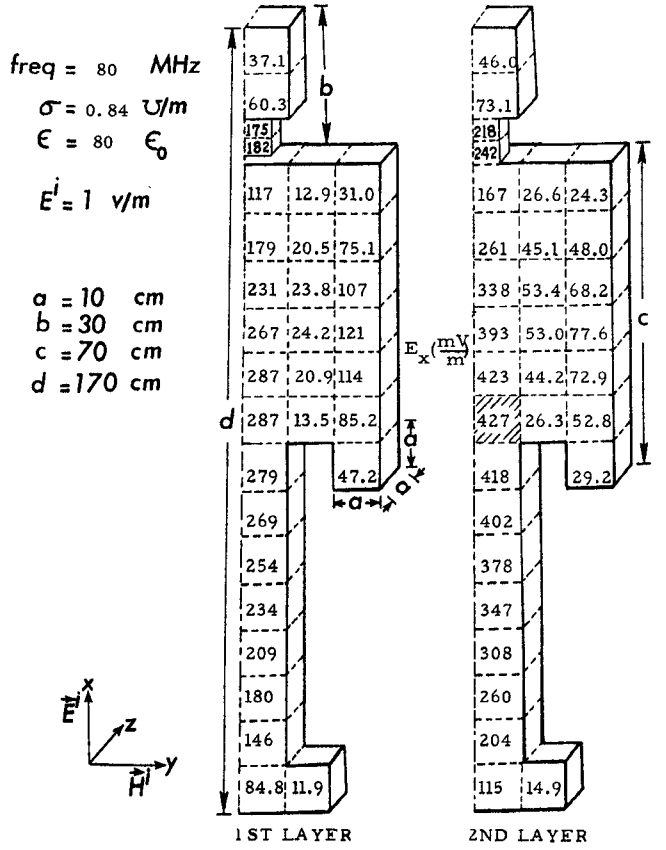

Fig. 12. The x component of an electric field induced inside a human torso with a thin neck by a vertically polarized EM wave of 80 MHz with an incident electric field of 1 V/m. Note the local hot spot at the neck.

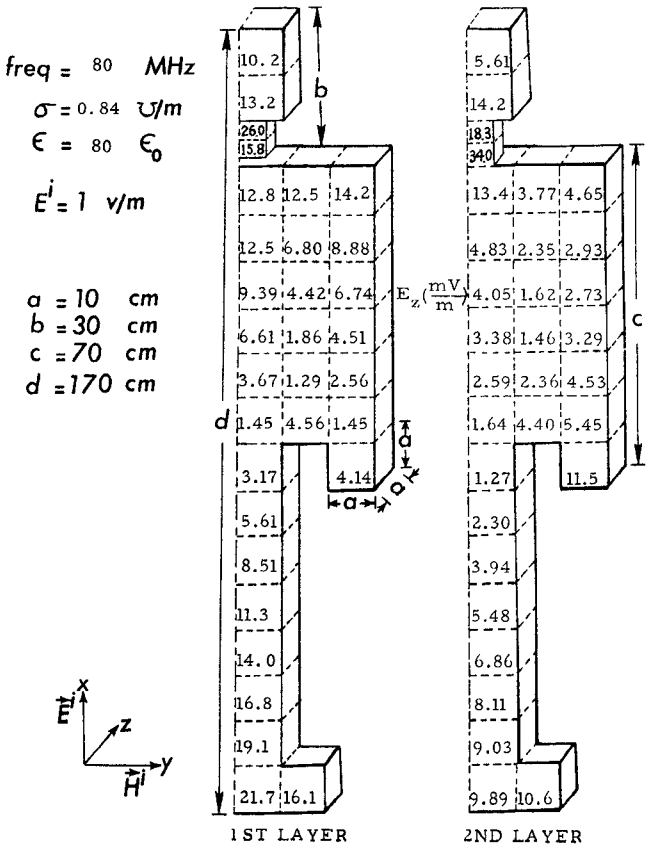

Fig. 14. The z component of an electric field induced inside a human torso with a thin neck by a vertically polarized EM wave of 80 MHz with an incident electric field of 1 V/m.

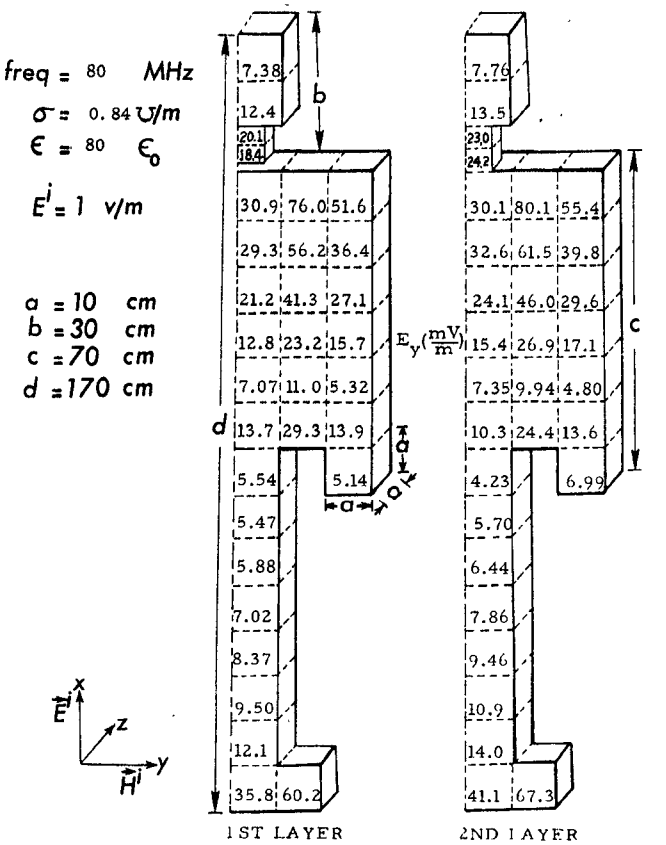

Fig. 13. The y component of an electric field induced inside a human torso with a thin neck by a vertically polarized EM wave of 80 MHz with an incident electric field of 1 V/m.

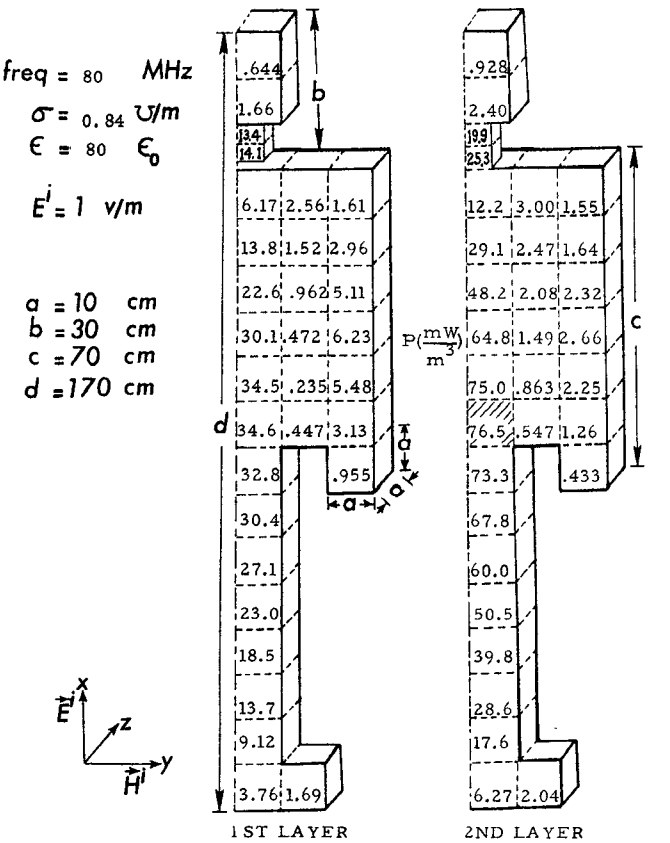

Fig. 15. The density of absorbed power induced inside a human torso with a thin neck by a vertically polarized EM wave of 80 MHz with an incident electric field of 1 V/m. Note the local hot spot at the neck.

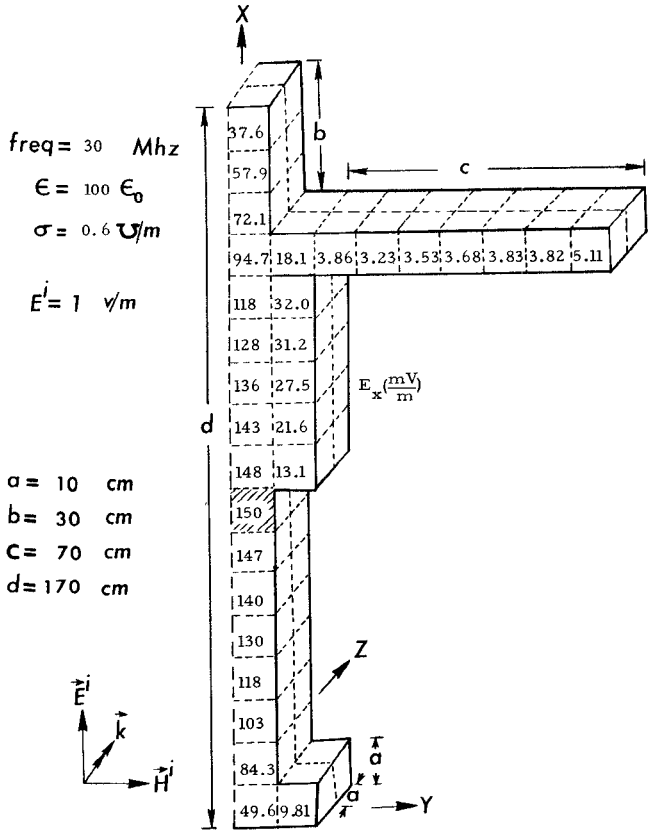

Fig. 16. The x component of an induced electric field in an adult torso with outstretched arms. Incident EM wave: vertical polarization, 30 MHz.

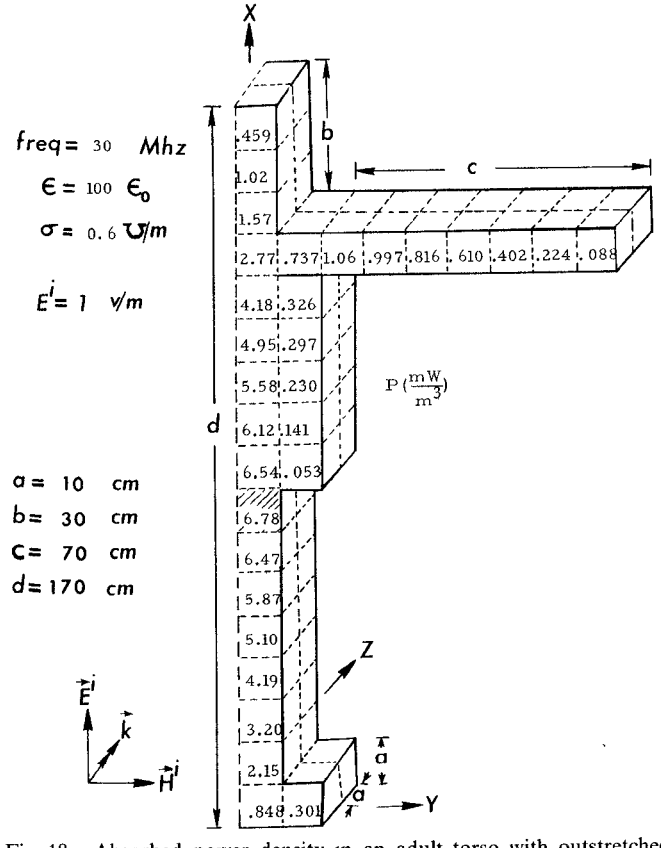

Fig. 18. Absorbed power density in an adult torso with outstretched arms. Incident EM wave: vertical polarization, 30 MHz.

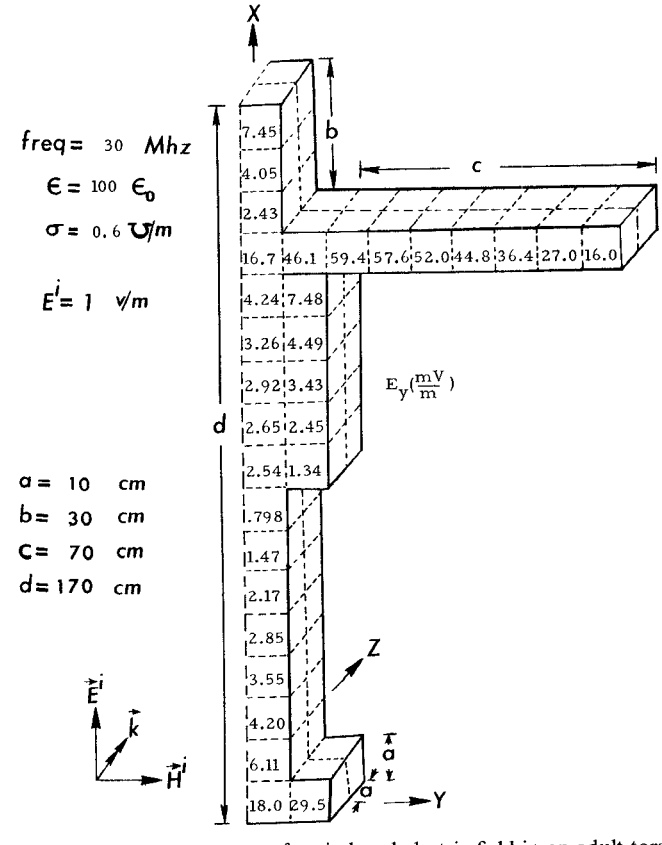

Fig. 17. The y component of an induced electric field in an adult torso with outstretched arms. Incident EM wave: vertical polarization, 30 MHz.

the induced electric field is not shown here because it is quite small compared with the other components. It is also noted that only the induced fields in the front layer are shown because the induced fields in the back layer are nearly the same as that in the front layer at this low frequency. When the results shown in Figs. 16–18 are compared with the corresponding results in the previous torso, as shown in Figs. 19–21, it is observed that the distributions of the induced fields are significantly changed, especially the y component of the induced electric field in the arms. This change is reasonable because the geometry of the second modified torso is significantly different from the previous torso and the outstretched arms now provide a good path for the horizontal component of the induced current.

The third modified torso is a child's torso with a height of 1.02 m and a shape as shown in Fig. 22. This torso is assumed to be illuminated by a vertically polarized EM wave of 80 MHz with a unity incident electric field. The x component of the induced electric field and the absorbed power density are shown in Figs. 22 and 23, respectively. When these results are compared with the corresponding results in an adult torso 1.7 m in height, as shown in Figs. 3 and 6, significant changes are observed between these two cases. The induced fields in the child torso are considerably smaller than those in the adult torso. The location of the maximum induced field in the child torso appears in the groin region of the front layer of the torso. It is noted that the induced fields in a child torso can be stronger than that in an adult torso if the frequency of the incident EM becomes higher [11].

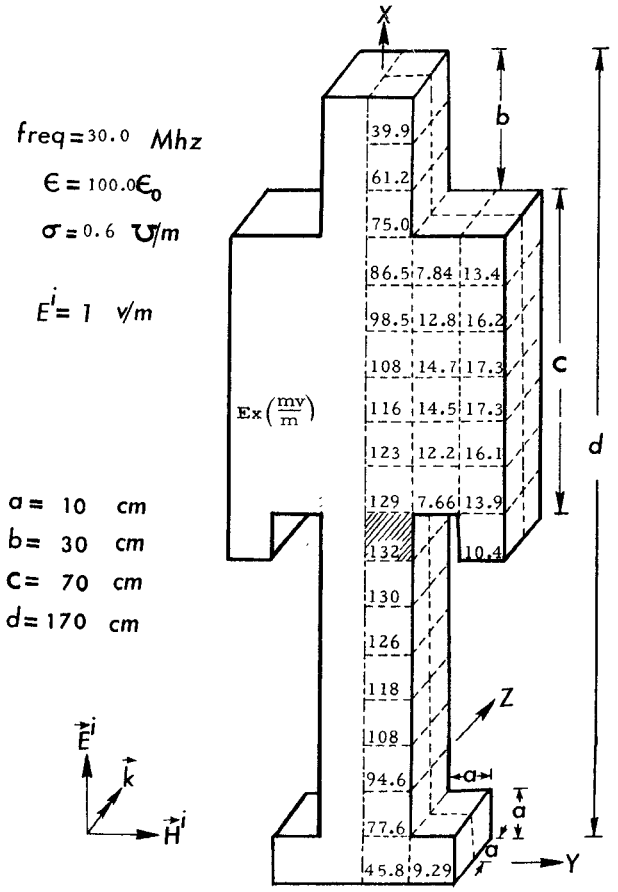

Fig. 19. The x component of an induced electric field inside an adult torso. Incident EM wave: vertical polarization, 30 MHz.

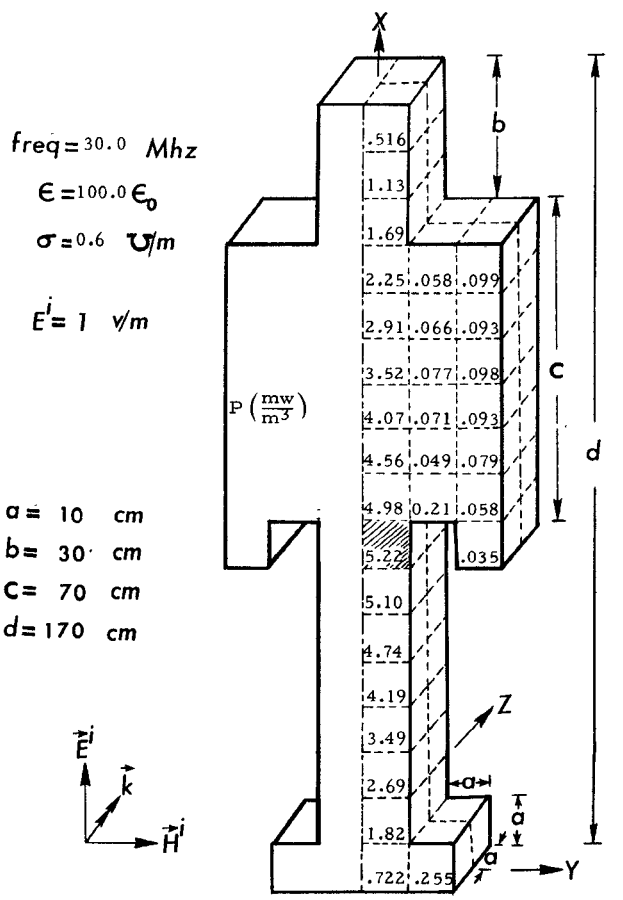

Fig. 21. Absorbed power density inside an adult torso. Incident EM wave: vertical polarization, 30 MHz.

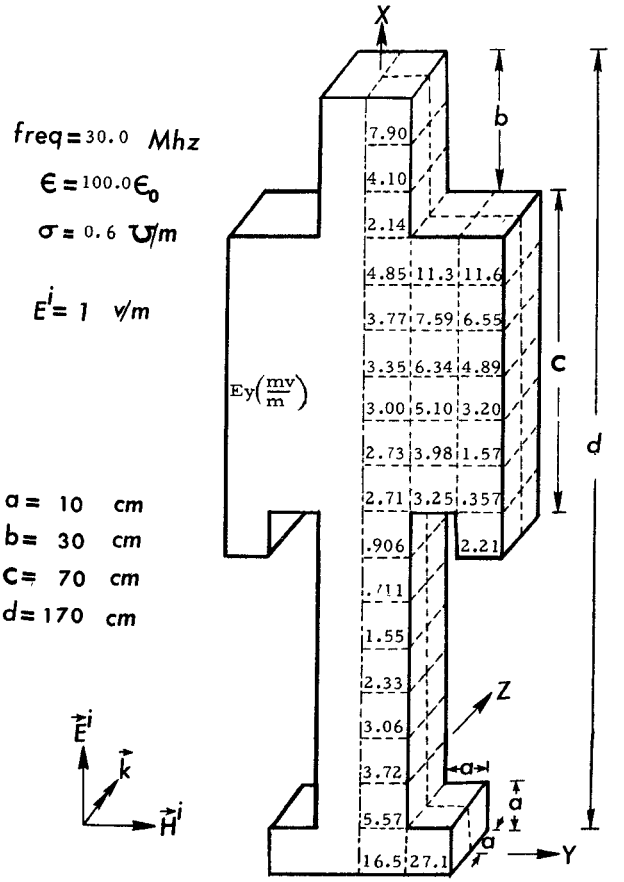

Fig. 20. The y component of an induced electric field inside an adult torso. Incident EM wave: vertical polarization, 30 MHz.

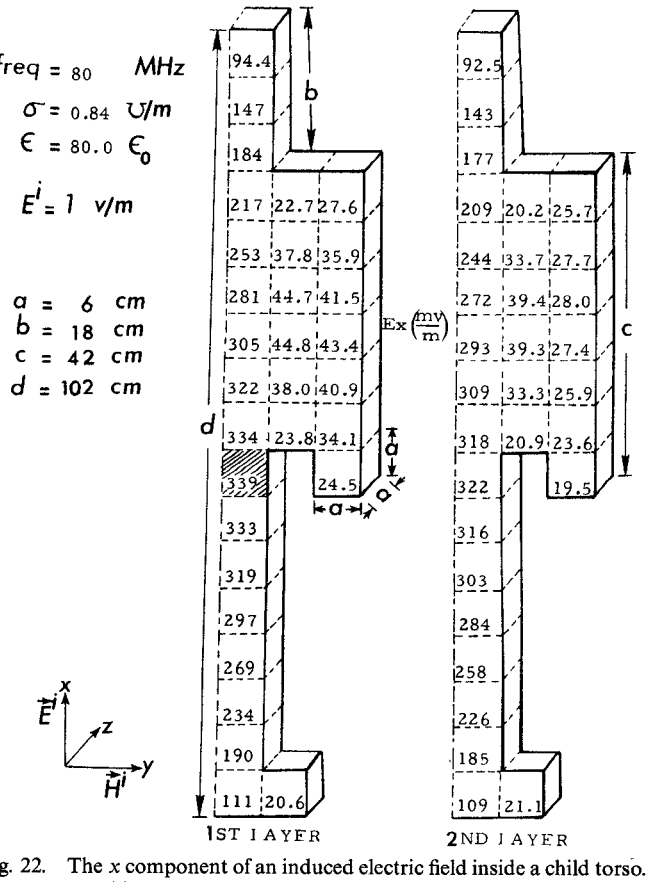

Fig. 22. The x component of an induced electric field inside a child torso. Incident EM wave: vertical polarization, 80 MHz.

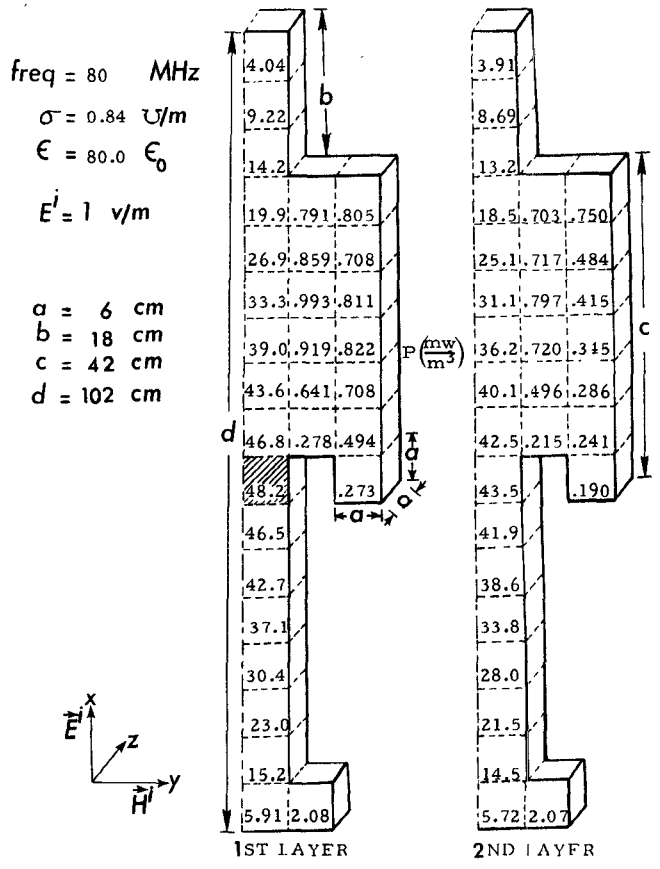

Fig. 23. Absorbed power density inside a child torso. Incident EM wave: vertical polarization, 80 MHz.

IV. Comparison with Existing Experimental Results

Theoretical results on the induced fields inside a typical adult torso presented in the preceding section were compared with existing experimental results of Gandhi [12] and a good qualitative agreement was obtained. The comparisons of some theoretical results with major experimental findings of Gandhi are summarized in Table I for the case of an adult torso illuminated by vertically polarized EM waves.

It is noted that the total absorbed power is expressed in terms of a different quantity by Gandhi in his paper. He used the relative absorption coefficient S which was defined as [(total absorbed power/incident power density)/physical-shadow area)]. In this paper, S is equal to $3.742A_r$, where A_r is the relative absorption area as defined in Section III-B.

Gandhi obtained his experimental results mainly on a scaled-down phantom figurine 18.4 cm in length and mice exposed to 710–3000-MHz EM waves. Since the geometries of the experimental and theoretical models used in our study are not very similar, the qualitative agreement shown in Table I is considered to be quite satisfactory.

V. Discussion

This paper presents some theoretical results on the internal electric field and absorbed power density induced by EM waves of various frequencies and polarizations inside typical human torsos. Extensive results for other frequencies are available in a recently published report [11] and can be obtained from the authors.

TABLE I
Comparisons of Some Theoretical Results with Experimental Results of Gandhi on Induced Fields Inside an Adult Torso Illuminated by Vertically Polarized EM Waves

	Theoretical Results (Tensor Int. Eq. Method)	Experimental Results (Gandhi's exp.)
Resonant length of torso (L)	$L/\lambda_0 = 0.453$	$L/\lambda_0 \approx 0.4$
Resonant frequency for an adult torso	f = 80 MHz (for L = 1.7m)	f = 65 ∿ 75 MHz (for L = 1.75m)
Effective absorption area at resonance	3 (3.742 Ar)	3 ∿ 4
Hot spot	local hot spot at neck area	hot spot at neck area

It is noted that in some cases there is a great jump in the induced field between adjacent cells such as in Fig. 3. This phenomenon can occur only between adjacent cells where no continuity of the induced current is required. For example, E_x in Fig. 3 can jump greatly from one cell in one column to the adjacent cell in the next column. However, no such jump is observed in the adjacent cells in the same column because of the continuity of the induced current. The great jump between one column to the next column indicates a strong standing wave pattern of the induced field inside the torso. This phenomenon was observed experimentally also [10].

In the course of our numerical computation, it was observed that the induced fields are quite sensitive to the torso geometry, especially in narrow or thin regions of the torso. For this reason, we plan to calculate the induced fields in a more realistic torso model in the future.

References

[1] H. P. Schwan, "Radiation biology, medical applications, and radiation hazards," in *Microwave Power Engineering*, vol. 2, E. C. Okress, Ed. New York: Academic Press, 1968, pp. 215–232.

[2] J. F. Lehmann, A. W. Guy, V. C. Johnston, G. D. Brunner, and J. W. Bell, "Comparison of relative heating patterns produced in tissues by exposure to microwave energy at frequencies of 2450 and 900 megacycles," *Arch. Phys. Med. Rehabil.*, vol. 43, pp. 69–76, Feb. 1962.

[3] A. R. Shapiro, R. F. Lutomirski, and H. T. Yura, "Induced fields and heating within a cranial structure irradiated by an electromagnetic plane wave," *IEEE Trans. Microwave Theory Tech.*, vol. MTT-19, pp. 187–196, Feb. 1971.

[4] H. N. Kritikos and H. P. Schwan, "Hot spots generated in conducting spheres by electromagnetic waves and biological implications," *IEEE Trans. Biomed. Eng.*, vol. BME-19, pp. 53–58, Jan. 1972.

[5] J. C. Lin, A. W. Guy, and C. C. Johnson, "Power deposition in a spherical model of man exposed to 1–20 MHz electromagnetic field," *IEEE Trans. Microwave Theory Tech.*, vol. MTT-21, pp. 791–797, Dec. 1973.

[6] H. S. Ho, A. W. Guy, R. A. Sigelmann, and J. F. Lehmann, "Electromagnetic heating patterns in circular cylindrical models of human tissue," in *Proc. 8th Annu. Conf. Medical and Biological Engineering*, p. 27 (Chicago, IL, July 1969).

[7] C. H. Durney, C. C. Johnson, and H. Massoudi, "Long-wavelength analysis of plane wave irradiation of a prolate spheroid model of man," *IEEE Trans. Microwave Theory Tech.*, vol. MTT-23, pp. 246–253, Feb. 1975.

[8] C. C. Johnson, C. H. Durney, and H. Massoudi, "Long-wavelength electromagnetic power absorption in prolate spheroidal models of man and animals," *IEEE Trans. Microwave Theory Tech.*, vol. MTT-23, pp. 739–747, Sept. 1975.

[9] D. E. Livesay and K.-M. Chen, "Electromagnetic fields induced inside arbitrarily shaped biological bodies," *IEEE Trans. Microwave Theory Tech.*, vol. MTT-22, pp. 1273–1280, Dec. 1974.

[10] B. S. Guru and K.-M. Chen, "Experimental and theoretical studies

on electromagnetic fields induced inside finite biological bodies," *IEEE Trans. Microwave Theory Tech.*, vol. MTT-24, pp. 433–440, July 1976.
[11] K.-M. Chen and B. S. Guru, "Internal EM field and absorbed power density inside human torsos induced by 1 to 500 MHz EM waves," Division of Engineering Research, Michigan State University, East Lansing, MI, NSF Tech. Rep., 1976.
[12] O. P. Gandhi, "Condition of strongest electromagnetic power deposition in man and animals," *IEEE Trans. Microwave Theory Tech.*, vol. MTT-23, pp. 1021–1029, Dec. 1975.

Modal Characteristics of Crossed Rectangular Waveguides

FENG-LING CHENG LIN

Abstract—**The modal solution for the crossed rectangular waveguide is presented. Cutoff frequencies and modal fields are determined by formulating an integral eigenvalue equation which can be solved by application of the Ritz–Galerkin method. Field equations are given for both TE and TM modes. The calculated cutoff frequencies of several lower order modes agree very well with the available experimental results in the literature.**

I. Introduction

In PHASED ARRAY antenna systems, open-ended waveguides are commonly used as the radiating elements. In order to provide dual-polarization capability, circular or square waveguides are used because they can support two orthogonal modes [1]. In addition, a wide bandwidth is required for the propagation of the dominant mode.

It has been known for years that ridged waveguides have been useful in microwave systems due to their wide bandwidth properties. For double-ridged waveguide, the TE_{10}-TE_{20} modal bandwidth is increased with the ridge loading. However, a system capable of operating in two polarizations is desirable in practical applications. Thus the waveguide with a 90° rotational symmetry is adopted. Chen *et al.* [2] have performed detailed modal analysis on quadruple-ridged circular and square waveguides by means of Silvester's finite element program [3]. It was shown that for square waveguides, quadruple-ridged loading always decreases the TE_{10}–TE_{11} bandwidth, whereas for circular waveguides, a finite amount of additional separation between TE_{11} and TM_{01} modes can be achieved when the ridge dimensions are chosen properly.

The crossed rectangular waveguide possesses 90° rotational symmetry, thus providing dual-polarization properties. It can also be viewed as ridged waveguide with square ridges loading its corners. It is of physical interest to investigate the modal characteristics and to determine the cutoff frequencies and the transverse field patterns.

With the complete knowledge of the waveguide's eigenvalue spectrum, one can solve many problems currently encountered. One such problem for instance, is the radiation of crossed rectangular waveguide elements in an array environment where excitation of asymmetrical higher order modes may create blind spots in the array scan pattern. Another problem is to predict the transmission characteristics of a plane wave incident at any arbitrary angle through an infinitely thin conducting sheet perforated periodically with crossed rectangular shaped apertures. The latter is particularly useful in the design and development of dichroic subreflectors for ground station and spacecraft antenna systems [4].

Modes of crossed rectangular waveguide have been determined by Stalzer *et al.* [5] with the aid of a computer program developed by Konrad and Silvester [6] using the triangular finite element method. In their studies, the transverse fields for each mode can not be obtained in explicit forms for further numerical manipulation. The Ritz–Galerkin method [7] has been successfully applied by Montgomery [8] to obtain the complete eigenvalue solution of dual-ridged waveguides. In this paper an integral-eigenvalue problem is formulated for the crossed rectangular waveguide and solved numerically by applying the Ritz–Galerkin method. The modal fields obtained are in the form of Fourier series which can be conveniently used for phased array analysis and aperture reflection coefficient determination for a waveguide element in an infinite array environment.

Manuscript received June 28, 1976; revised March 22, 1977. This research was supported by the National Aeronautics and Space Administration under contract NAS5-23000.

The author is with Sachs/Freeman Associates, Inc., Hyattsville, MD 20784, for Johns Hopkins University Applied Physics Laboratory, Laurel, MD 20810.

II. Theoretical Formulation

The geometry of the crossed rectangular waveguide is shown in Fig. 1. The plane $x = 0$ is a symmetry plane of the waveguide and the field is calculated for only half of the cross